Update of the neutrino and photon limits from the Pierre Auger Observatory

C. Bleve [1,2], G. Cataldi[2], M. R. Coluccia[1,2], I. De Mitri[1,2], G. Marsella[1,2], D. Martello[1,2], L.Perrone[1,2], V. Scherini[1,2]

[1] Dipartimento di Matematica e Fisica "Ennio De Giorgi", Università del Salento, Italy
[2] Istituto Nazionale di Fisica Nucleare sez. di Lecce, Italy

1. Abstract

Ultra-high energy neutrinos and photons, with energies above 1 EeV and 10 EeV respectively, can be detected with the Surface Detector array (SD) of the Pierre Auger Observatory. Downward-going neutrinos of all flavours interacting in the atmosphere at zenith angles $\theta > 60°$, upward-going tau neutrinos ("Earth-skimming"), as well as photons in the zenith range $30° - 60°$ can be identified through the broad time-structure of the signals expected to be induced in the SD stations. An additional signature for photon-induced air showers is the steeper lateral distribution of secondary particles at ground with respect to the nucleonic showers. Stringent limits are set to the diffuse flux of ultra-high energy (UHE) neutrinos and photons, using data collected between 2004 and mid-2013, under the hypothesis of an E^{-2} spectrum for signal primaries.

2. Introduction

Searches for ultra-high energy (UHE) photons and neutrinos are amongst the methods used to unravel the mystery of the origin of cosmic rays of the highest energy. Protons and nuclei interacting with the universal low energy photon background (CMB) are expected to produce a flux of UHE photons that can propagate for a few tens of Mpc without being absorbed and neutrinos (from the decay of charged pions, muons and neutrons) that can travel to the observer with no interaction or deflection. The expected cosmogenic fluxes depend on the composition and maximum energy of CRs at the sources and the emissivity, distribution and cosmological evolution of the acceleration sites. Thus, observing UHE photons or neutrinos, can pose constraints on the UHECR origin and properties of the sources.
The Surface Detector array (SD) of the Pierre Auger Observatory covers ∼3,000 km^2 with a triangular grid of water-Cherenkov Detectors (WCD) [1] providing a very large exposure for the search of UHE neutrinos and photons. We report here upper limits to the diffuse fluxes obtained with the analysis of data collected between 2004 and mid-2013.

3. Search method

SD observables for the searches of neutrino and photons are identified on the base of the expected physical differences between signal and background, quantified using simulations of air showers initiated by signal particles. The background of showers induced by nuclei is not simulated, instead a fraction of the data set is used as a training sample to define the selection for candidate signal events. The search sample consists of the remaining events.

3.1. UHE neutrinos

The search for neutrinos exploits the extremely small cross-section of the signal particles. At large zenith angles ($\theta > 60°$) the thickness of the atmosphere traversed is large enough to absorb almost completely the electromagnetic component of showers initiated by nucleons or even photons, leaving their signal dominated by muons. Showers initiated by neutrinos very deep in the atmosphere, on the other hand, have a considerable amount of the electromagnetic component remaining ("young" showers). Two types of neutrino-induced showers are sought:
(1) Earth-Skimming (ES) showers ($90° < \theta < 95°$, induced by ν_τ travelling upward with respect to the vertical at the ground) can skim the crust of the Earth and interact close to the surface, producing a τ lepton which can decay in flight in the atmosphere close to the SD. At 10^{18} eV the mean decay length of the τ lepton is ∼50 km.
(2) Downward-Going (DG) showers ($60° < \theta < 90°$) initiated by neutrinos of all flavours interacting in the atmosphere close to the SD

through neutral current or charged current interactions, as well as showers produced by ν_τ interacting in the mountains surrounding the observatory.

The ν-nucleon interactions for DG neutrinos in the atmosphere are simulated with HERWIG [2]; the τ propagation in Earth and in the atmosphere with TAUOLA [3] (with ν-nucleon cross-section from [4]); the subsequent air shower is simulated with AIRES [5]. To identify neutrinos we search for very inclined "young" showers. Signatures of inclined showers are: large ratio length/width (L/W) of the major/minor axis of the ellipse encompassing the footprint of the shower (Fig. 1 (i)) and the distribution of apparent speeds of the trigger time between stations being required to have an average value close to the speed of light and a small RMS. Large values of the Area-over-Peak ratio (AoP, Fig. 1 (ii)) in the time traces indicate a large contribution of the electromagnetic component. For all the channels the observable used to identify neutrinos is generally based on the AoP of stations: the full selection strategy is described in [6]. The region for neutrino candidates is defined using a training data sample (∼20% of the whole data set). From the distribution of the data in the training set, the range of the separation variable in which 1 event is expected in 50 yr on the full SD array is defined. Any event in this range is considered as a neutrino candidate. Fig. 2 illustrates the exponential fit of the tail of the data distribution for the ES channel, using the average AoP of early stations as the discriminating variable [6]. The results on the search sample are also shown.

3.2. Photons (E_γ >10 EeV)

Showers induced by photons are characterised by a lower content of muons and larger average depth of maximum longitudinal development ($X_{\rm max}$) than showers initiated by nuclei with the same energy. This is due to the radiation length being more than two orders of magnitude smaller than the mean free path for photo-nuclear interaction, causing a reduced transfer of energy to the hadron/muon channel, and to the development of the shower being delayed by the typically small multiplicity of electromagnetic interactions. The Landau-Pomeranchuk-Migdal (LPM) effect becomes important beyond 10 EeV. At E_γ >50 EeV - for the site of the Pierre Auger Observatory - photons can also convert in the geomagnetic field producing a pre-shower [7], with the probability of this occurring increasing with energy and depending on the arrival direction with respect to the field. The resulting air-shower is, in this case, a superposition of cascades initiated by lower en-

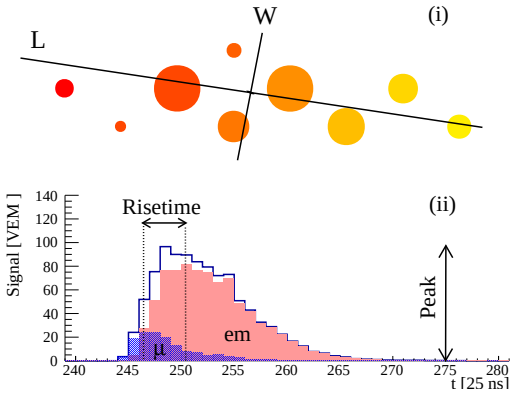

Figure 1. The footprint of an inclined event (i) on the SD detector: colours from light to dark represent trigger times from early to late, circle areas are proportional to the logarithm of the total signal in individual stations. L, the direction of arrival projected on the detector plane, is the major axis of the ellipse encompassing the footprint, W the minor axis. An example of a time trace in a SD station digitised with a FADC in 25 ns bins is shown in (ii): a larger fraction of electromagnetic (em) signal produces a larger Area over Peak (AoP) ratio and a larger risetime.

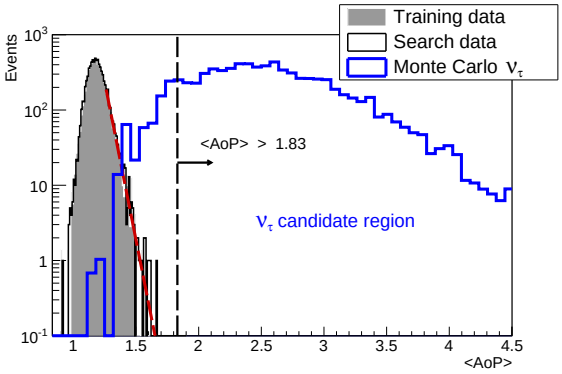

Figure 2. Distributions of ⟨AoP⟩ (the variable used to identify neutrinos in the ES selection for data after 01/06/2010) after applying the inclined shower selection. The distributions for data in the training period (full grey histogram) and search period (black histogram) are normalised to the same number of events. The blue histogram shows the simulated ES ν_τ events. The vertical line represents the cut on ⟨AoP⟩ above which an event is regarded as a neutrino candidate. An exponential fit to the tail of the distribution of training data is also shown as a red dashed line - see text for details.

ergy electrons and photons with smaller $\langle X_{\rm max}\rangle$ and larger ratio of muonic to electromagnetic content, at ground level, than showers induced by non-converted photons of the same energy [8].
The effects of pre-shower and LPM are both included in the simulations of photon showers used for this analysis, generated with an energy spectrum E^{-1}. Air showers are simulated with CORSIKA [9] (including PRESHOWER [10]), with QGSjetII.03 [11] as hadronic generator.
Photons are searched for in the $30^\circ < \theta < 60^\circ$ zenith range[1], the reconstruction of the energy-related observable $S(1000)$, the signal in VEM (vertical equivalent muons) at 1000 m from the shower axis, is the same as for the SD spectrum analysis [12], where the function used to fit the lateral distribution of the signal (LDF) has a shape parameterised to describe the bulk of Auger data. The conversion of ($S(1000)$,θ) to energy is specific for the photon search. An iterative procedure similar to the one described in [13] is used, assuming the universality of $S(1000)/E^\alpha$ as a function of $DX = X_{\rm obs} - X_{\rm max}$ (DX is the difference in atmospheric depth between the observation level and the shower $X_{\rm max}$, used as an indicator of the shower age, i.e. stage of development of the cascade). To avoid analysing showers not fully developed, we require $X_{\rm max}$ to be no more than 50 g cm^{-2} below the ground level ($DX > -50$ g cm^{-2}). The universal profile is described with a Gaisser-Hillas function whose parameters, together with α, are calibrated with photon simulations.
The reduced muon content of photon showers with respect to data ($\sim$ 15% compared to protons at 10 EeV, for QGSjetII.03) produces a steeper lateral distribution of the signal observed in WCDs at ground level. At large distances from the axis, photon showers produce typically smaller signals than expected from the data LDF (Fig. 3 (i)). We thus define an event observable measuring the departure from the average data LDF as the logarithm of the average deviation of the station signal from the event LDF: $L_{LDF} = log_{10}(\frac{1}{N}\sum_i S_i/LDF(r_i))$ where i runs over the stations with radial distance from the shower axis $r_i > 1000$ m, S_i is the total signal of the i-th station, $LDF(r_i)$ is the signal value at distance r_i according to the LDF fit. L_{LDF} is expected to be negative for photons.
The spread in the arrival time of secondary particles in individual stations can be measured defining the risetime as the difference between the 50% and 10% time quantiles of the FADC time trace (Fig. 1 (ii) on page 2). The risetime is not only increased by a larger contribution of the electromagnetic component, it also increases when the difference in depth between $X_{\rm max}$ and the observation level becomes smaller, for geometrical reasons. Being sensitive to both the deeper $X_{\rm max}$ and limited muon content of photon showers, the risetime is a suitable variable for the search of photons. The raw risetime is corrected for azimuthal asymmetry effects (i.e. difference between earlier and later triggering stations in an inclined event) obtaining $t_{1/2}$. The correction is based on the average effect observed in data. A "Data Benchmark" is produced to describe the average risetime of data. Sampling fluctuations, $\sigma_{t_{1/2}}$, are also estimated from the data, using the difference of the measurements of station doublets (a station in the regular SD grid plus a second station off-grid deployed close to it) or station pairs (two stations in the same event with similar distance from the axis and total signal). For each station, $\delta_i = (t^i_{1/2} - t^{Bench}_{1/2})/\sigma^i_{t_{1/2}}$ measures the deviation of the corrected risetime of the station from the data benchmark in units of expected standard deviation (Fig. 3 (ii)). For photon searches an event observable $\Delta = (\sum_i \delta_i)/N$ is defined, where the sum runs over stations with $S > 6$ VEM, and radial distance in the range 600-2000 m. A minimum of 4 selected stations is required. Δ is expected to average $\sim$0 for data and to be significantly positive for air showers initiated by photons.
The observables L_{LDF} and Δ are redefined to obtain a distribution with mean zero and standard deviation 1 for photon showers. Taking $x = L_{LDF}$ or $x = \Delta$, we define: $gx = (x - \bar{x}_\gamma(E_\gamma,\theta))/\sigma_\gamma(E_\gamma,\theta)$. The resulting distribution is shown in Fig. 4 for the training data set (grey) consisting of 2% of data, and photon simulations (red). Only events with reconstructed photon energy > 10 EeV, and photons not converting in the geomagnetic field are considered[2]. A Principal Component Analysis (PCA) on the training data set and unweighted photon simulations defines the first component, used for the selection of photon candidate events (Fig. 4). Its distribution is shown in Fig. 5 for the search data set

[1]The $\langle X_{\rm max}\rangle$ of photons at 10 EeV is already $\sim$ 100 g cm^{-2} larger than the atmospheric vertical depth at the site. Selecting a minimum zenith of 30° (observation depth $\simeq$1020 g cm^{-2}) guarantees that most UHE photon-induced showers are fully developed at the depth of observation.

[2] The distribution of the observables is different for photons pre-showering or not, as a consequence of the differences in $\langle X_{\rm max}\rangle$ and ratio of muonic to electromagnetic signal at ground. Non-preshowering photons initiate cascades from the interaction of a primary photon with the atmosphere and they are the larger subset in the energy range considered (relative contributions are visible in Fig. 5).

(98% of data collected between 01/01/2004 and 15/05/2013) and photon simulations weighted to an E^{-2} spectrum. The photon candidate cut is defined, with an "a priori" choice, to be the value of the median of the weighted distribution of non-pre-showering photon simulations. Any event with principal component larger than the median cut value is considered as a photon candidate.

4. Results

After application of the selection criteria to the data, no event collected between 01/01/2004 and 20/06/2013 is selected with the neutrino cuts, while 4 events survive the photon cuts in the period between 01/01/2004 and 15/05/2013. The corresponding exposure is determined by application of the same criteria to simulated showers induced by signal primaries. Assuming a differential flux $dN(E) = k \cdot E^{-2}$ for both neutrinos and photons, upper limits to their flux are derived.

4.1. Limits to the flux of neutrinos

An upper limit on the value of k is obtained at a confidence level CL:

$$k_\nu^{\rm CL} = \frac{N_\nu^{\rm CL}}{\int_{E_\nu} E_\nu^{-2} \mathcal{E}_{\rm tot}(E_\nu) dE_\nu} \qquad (1)$$

where $N_\nu^{\rm CL}$ is the upper limit at confidence level CL to the number of neutrino events, assuming conservatively that no background event is expected. $N_\nu^{\rm CL}$ is determined from the number of candidates using a semi-Bayesian extension [14] of the Feldman-Cousins approach [15] to include the uncertainties in the calculation of the exposure $\mathcal{E}_{\rm tot}(E_\nu)$ combined for all the search channels. The relative contribution of the selection channels to the total expected event rate is ES:DG$\sim$0.84:0.16, under the hypothesis $\nu_e : \nu_\mu : \nu_\tau = 1 : 1 : 1$. Details of the neutrino exposure calculation and values as a function of E_ν are reported in [6]. The single-flavour limit to the normalisation factor of the diffuse flux of neutrinos is:

$$k_\nu^{90\%} < 6.4 \times 10^{-9}\ {\rm GeV\ cm^{-2}\ s^{-1}\ sr^{-1}}$$

for $E_\nu = 0.1 - 25$ EeV, defined as the energy range containing symmetrically 90% of the expected events for an E_ν^{-2} flux. An extensive study of systematic uncertainties is included [6].

The SD of the Auger Observatory is the first air shower array to set a limit below the Waxman-Bahcall bound [19]. As shown in Fig. 6, cosmogenic ν models that assume a pure primary proton composition at the sources for strong evolution (FRII-type) of the sources [17] and constrained by the GeV observations of Fermi-LAT

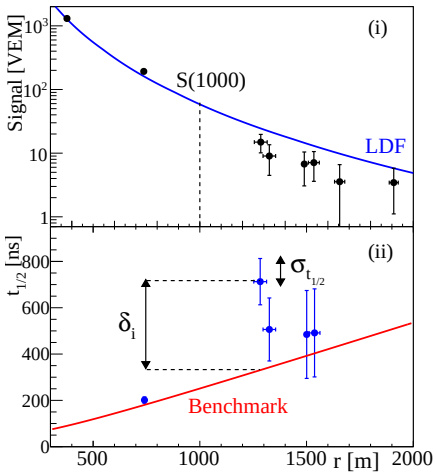

Figure 3. A shower induced by a photon of $\sim$20 EeV simulated with a zenith angle of 45°: (i) the lateral distribution of signals in the WCDs is steeper than the LDF obtained from data (solid line) and (ii) the risetime of selected stations is larger than the average data benchmark (solid line) - see text for details.

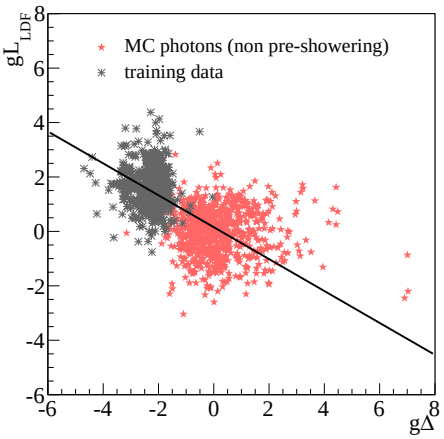

Figure 4. Principal component analysis for the photon search. The training data sample and a set of simulated photons, not undergoing pre-showering, are used to find the principal component (black line), i.e. the linear combination of gΔ and gL_{LDF} that maximises the separation of the two sets. The principal component is used as separation variable for the photon search.

[16] are disfavoured. The current Auger limit is approaching the fluxes predicted under a range of assumptions for the composition of the primary flux, source evolution and model for the transition from galactic to extragalactic cosmic-rays [

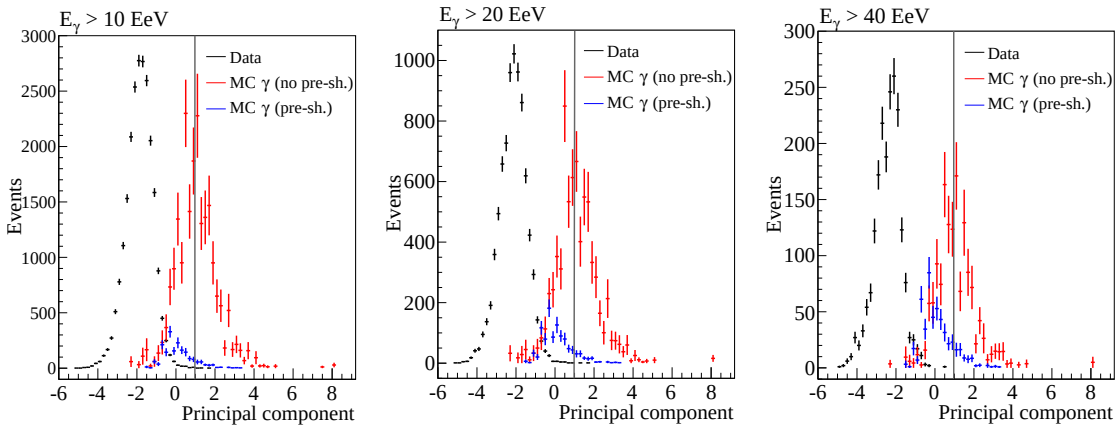

Figure 5. Photon search: distributions of the principal component for events in the search sample (black) photons non pre-showering (red) and pre-showering (blue) for three different energy thresholds. Photon simulations are weighted to an E^{-2} spectrum and the median of the non pre-showering photon distribution is defined as the photon candidate cut (vertical line). The photon distribution is normalised to the number of data. Only 4, 2, 0 events survive the selection.

18]. A 10-fold increase in the exposure will be needed to reach the most optimistic predictions in case of a pure iron composition at sources, out of the range of the current configuration of the observatory.

4.2. Limits to the integrated photon flux

The upper limits on the integral flux of photons, for $E_\gamma > E_0$, are defined as:

$$F_\gamma^{\rm CL}(E_\gamma > E_0) = \frac{N_\gamma^{\rm CL}}{\langle \mathcal{E} \rangle} \qquad (2)$$

where E_γ is assigned according to the photon energy reconstruction; $N_\gamma^{\rm CL}$ is the Feldman-Cousins upper limit to the number of photon events computed at a confidence level CL in the hypothesis of no background event expected; $\langle \mathcal{E} \rangle$ is the spectrum-weighted average exposure in the energy range $E_\gamma > E_0$. In the period of data taking considered, the value of $\langle \mathcal{E} \rangle$ is 5200, 6800, 6300 km^2 sr yr, for E_γ >10, 20, 40 EeV respectively. The limits to the integral flux are:

$$F_\gamma^{95\%}(E_\gamma > 10,\ 20,\ 40\ {\rm EeV}) < 1.9,\ 1.0,\ 0.49 \times 10^{-3}\ {\rm km}^{-2}\ {\rm yr}^{-1}\ {\rm sr}^{-1}.$$

The limits to the diffuse flux of photons obtained with the Auger Observatory are the most stringent currently available above 1 EeV (Fig. 7). Top-down models of photon production from the decay of heavy primordial particles [27, 28] are strongly disfavoured. Preliminary limits derived in this work for $E_\gamma > 10$ EeV start constraining the most optimistic predictions of cosmogenic photon fluxes in the assumption of a pure proton composition at the sources [27]. Cosmogenic models using a primary spectral index of -2 and maximum energy of 10^{21} eV at the sources [17] predict an integrated photon flux above 10 EeV ∼4 times lower than the current limits in the case of proton primaries, ∼2 orders of magnitude lower if iron nuclei are injected at the sources.

REFERENCES

1. The Pierre Auger Collaboration, Nucl. Instrum. Meth. A 798, (2015) 172
2. G. Corcella *et al.*, HERWIG 6.5, *JHEP* **01** (2001) 010 [arXiv:hep-ph/0012319].
3. S. Jadach *et al.*, *Comput. Phys. Commun.* **76** (1993) 361.
4. A. Cooper-Sarkar, S. Sarkar, *JHEP* **0801** (2008) 075 [arXiv:0710.5303].
5. S. J. Sciutto, arXiv:astro-ph/9911331,
6. The Pierre Auger Collaboration, *Phys. Rev. D* **91** (2015) 092008 [arXiv:1504.05397].
7. B. McBreen and C. J. Lambert, *Phys. Rev. D*, **24** (1981) 2536.
8. P. Homola *et al.*, *Astropart. Phys.* **27** (2007) 174 [arXiv:astro-ph/0608101].
9. D. Heck *et al.*, Report FZKA **6019** (1998).
10. P. Homola *et al.*, *Comput. Phys. Comm.* **173** (2005) 71 [arXiv:astro-ph/0311442].
11. S. Ostapchenko, *Phys. Lett. B* **636** (2006) 40 [arXiv:hep-ph/0602139].
12. The Pierre Auger Collaboration, *Phys. Rev. Lett.* **101** (2008) 061101 [arXiv:0806.4302]; The Pierre Auger Collaboration, *Phys. Lett. B* **685** (2010) 239 [arXiv:1002.1975].
13. P. Billoir *et al.* arXiv:astro-ph/0701583.
14. J. Conrad *et al.*, *Phys. Rev. D* **67** (2003) 012002 [arXiv:hep-ex/0206034].

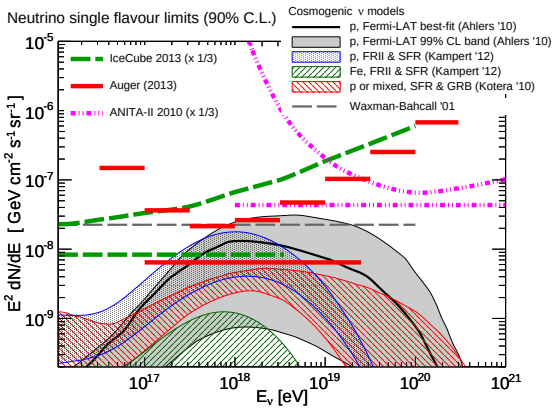

Figure 6. Upper limits to the diffuse flux of UHE neutrinos at 90% C.L. in integrated (horizontal lines) and differential form. Limits described in this work (red lines) are compared with cosmogenic neutrino models [16, 17, 18], the Waxman-Bahcall bound [19], and limits from IceCube [20] and ANITA [21]. All neutrino limits and fluxes are converted to single-flavour.

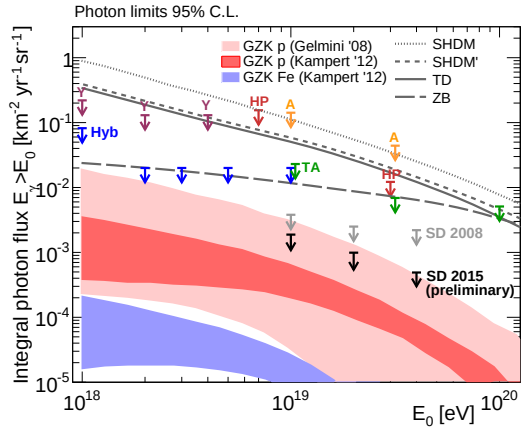

Figure 7. Upper limits at 95% C.L. to the diffuse flux of UHE photons derived in this work (black) shown together with previous results from the Pierre Auger Observatory with hybrid (Hyb) and SD data [22], Telescope Array (TA) [23], Yakutsk (Y) [24], Haverah Park (HP) [25], AGASA (A) [26] and predictions from several top-down [27, 28] and cosmogenic photon models [27, 17].

15. G. J. Feldman, R. D. Cousins, *Phys. Rev. D* **57** (1998) 3873 [arXiv:physics/9711021].
16. M. Ahlers *et al.*, *Astropart. Phys.* **34** (2010) 106 [arXiv:1005.2620].
17. K. -H. Kampert, M. Unger, *Astropart. Phys.* **35** (2012) 660 [arXiv:1201.0018];
    B. Sarkar *et al.*, Proc. 32nd ICRC Beijing, China **2** (2011) 198.
18. K. Kotera *et al.*, *JCAP* **10** (2010) 013 [arXiv:1009.1382].
19. J. Bahcall and E. Waxman, *Phys. Rev. D* **64** (2001) 023002 [arXiv:hep-ph/9902383].
20. The IceCube Collaboration, *Phys. Rev. D* **88** (2013) 112008 [arXiv:1312.0104].
21. The ANITA Collaboration, *Phys. Rev. D* **85** (2012) 049901(E) [arXiv:1011.5004].
22. The Pierre Auger Collaboration, *Astropart. Phys.* **29** (2008) 243 [arXiv:0712.1147];
    The Pierre Auger Collaboration, *Astropart. Phys.* **27** (2007) 155 [arXiv:astro-ph/0606619];
    The Pierre Auger Collaboration, *Astropart. Phys.* **31** (2009) 399 [arXiv:0903.1127];
    M. Settimo, for the Pierre Auger Collaboration, Proc. of 32nd ICRC, Beijing, China **2** (2011) 55 [arXiv:1107.4805].
23. The Telescope Array Collaboration, *Phys. Rev. D* **88** (2013) 112005 [arXiv:1304.5614].
24. The Yakutsk Collaboration, *Phys. Rev. D* **82** (2010) 041101 [arXiv:0907.0374].
25. M. Ave *et al.*, *Phys. Rev. Lett.* **85** (2000) 2244 [arXiv:astro-ph/0007386]
    and private communication from R. Vazquez, A. A. Watson, E. Zas.
26. The AGASA Collaboration, *Astroph. J.* **571** (2002) L117.
27. G. Gelmini, O. Kalashev, D. Semikoz, *JETP* **106** (2008) 1061 [arXiv:astro-ph/0506128].
28. J. Ellis, V. E. Mayes, D. V. Nanopoulos, *Phys. Rev. D* **74** (2006) 115003 [arXiv:astro-ph/0512303].